A SYSTEMATIC STUDY OF THE FAILURE WAVE PHENOMENON IN BRITTLE MATERIALS

Final Technical Report
by

G.I.Kanel, A.A.Bogatch, S.V.Razorenov, A.S.Savinykh
(April 2003)

United States Army

EUROPEAN RESEARCH OFFICE OF THE U.S. ARMY

London, England

CONTRACT NUMBER N62558-02-M-6020

Institute for High Energy Densities of Russian Academy of Sciences,
Izorskaya 13/19, Moscow, 127412 Russia

A SYSTEMATIC STUDY OF THE FAILURE WAVE PHENOMENON IN BRITTLE MATERIALS

Final Technical Report
by

G.I.Kanel, A.A.Bogatch, S.V.Razorenov, A.S.Savinykh
(April 2003)

United States Army

EUROPEAN RESEARCH OFFICE OF THE U.S. ARMY

London, England

CONTRACT NUMBER N62558-02-M-6020

Institute for High Energy Densities of Russian Academy of Sciences,
Izorskaya 13/19, Moscow, 127412 Russia

Contents

Abstract

Shock-wave experiments with four glasses of different hardness, two ceramics, quartz and silicon single crystals have been carried out with the goals to better understand in which materials the failure wave may occur under shock compression, which material properties control the formation and propagation, and what are the threshold conditions. Experiments with piles of thin sample plates confirm the appearance of the failure wave in elastically compressed fused quartz, K8 crown glass, and heavy flint glass, although the relationships between the Hugoniot elastic limits and the failure thresholds of these glasses are different. For softest heavy flint glass, the failure threshold is closest to the HEL. The failure waves were not recorded in single crystals and polycrystalline alumina and boron carbide ceramics. The results show that the propagation speed of the failure wave in glass slightly depends on the stress above the failure threshold, and does not depend on the propagation distance. The process becomes unstable and stops at stresses near the failure threshold. Longitudinal compressibility of comminuted glass has been found close to that of intact material. Preliminary results of computer simulations demonstrate the potential of the combustion-like model in simulating the evolution of failure wave.

1. Introduction

It is known that the behavior of brittle materials essentially differs from that of ductile metals and alloys [1]. Consequently, in order to use any tests for calibration of constitutive rheological models, one needs to know whether the observed response is brittle or ductile. However, until now we do not have trustworthy general criteria to recognize signatures of brittle response in measured histories of stress or particle velocity. As a result, it is not clear how valid the constitutive models of brittle materials are based on the shock wave tests. One of the manifestations of brittle response is the failure wave phenomenon that was observed in shock-compressed glasses. The failure wave is a network of cracks that are nucleated on the surface and propagate into the stressed body. Figure 1 presents the time-distance diagram which illustrates the phenomenon and its observations.

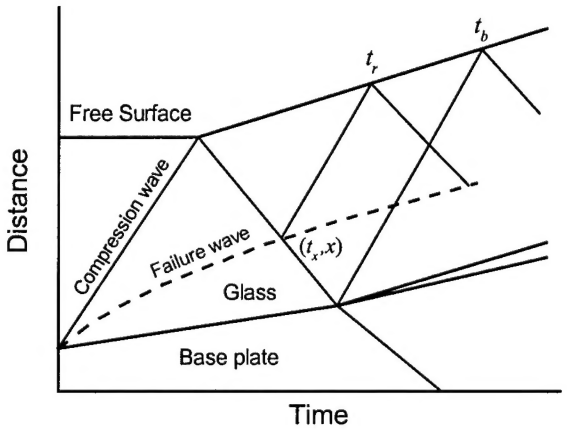

Figure 1. Distance-time diagram of shock-wave loading of a glass plate.

The experimental observations of the failure wave phenomena in shock-compressed glass may be summarized as follows:

(i) A decrease of deviator stresses and vanishing of the tensile strength occur behind the failure wave front.
(ii) Failure waves nucleate at a glass surface.
(iii) Failure waves are observed when the impact stress exceeds some threshold but is still below the Hugoniot elastic limit of glass.
(iv) Propagation of the failure wave stops when the stress decreases to a zero or nearly zero state.
(v) The failure wave velocity is much less than the sound speed.

Many measurements show that the failure wave speed is equal to an ultimate speed of growth of cracks (~1.5 km/s for glass), with higher or lower velocity values being observed. Both

constant and decreasing propagation velocities were reported. One may hope that the investigation of failure wave in shock-compressed glasses will provide information about the mechanisms and general rules of nucleation, growth and interactions of multiple cracks and lead to better understanding of experiments on other hard brittle materials, such as ceramics and rocks.

Our recent investigations [2] confirmed that the network of growing cracks in shock-compressed glass may indeed be considered as a failure wave which obeys the Rankine-Hugoniot conservation laws. It was shown that, when the failure wave is formed, shock compression of glass leads to a two-wave structure. Since the failure waves nucleate at each surface on each interface, the magnitude of the leading elastic wave in a pile of glass plates decreases as a result of its decomposition into two waves. The decrease of elastic wave amplitude should repeat at each interface until the failure threshold is reached. As a result, for a sufficiently large number of plates in the pile, an elastic precursor wave having an amplitude equal to the failure threshold should be formed. Figure 2 compares the free surface velocity histories recorded for single thick glass plate and for layered assemblies of 8 thin glass plates, subjected to the same impact loading [2]. The results show transformation of purely elastic compression wave followed by the failure wave in the single glass plate into the waveform which is typical for elastic–plastic solids in the pile of thin glass plates. The rise time of the second wave corresponds to approximately one-half of the time needed for the failure wave to pass through one plate. The final free surface velocity is practically equal to that of a single glass plate. The response of a layered assembly of thin brittle plates as compared to that of one thick plate is a simple way to diagnose nucleation of the failure process on the plate surfaces and determine the failure threshold.

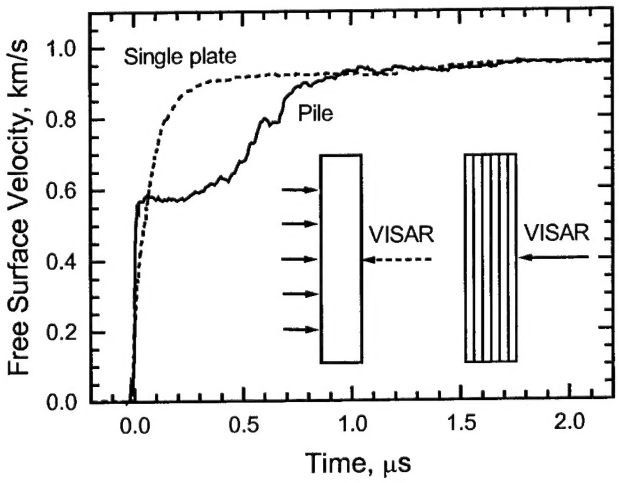

Figure 2. The free surface velocity histories recorded in shots with single thick glass plate and with pile of 8 glass plates of 1.21 mm average thickness [2].

The existing experimental data are not sufficient to say in which materials the failure wave may appear under shock compression, which material properties control the possibility of its appearance, what are the threshold conditions and how the kinematics parameters of the failure

waves depend on the stressed state. The failure threshold, the failure wave kinematics and stability, and the dynamic impedance of the matter behind the failure wave front are main tasks needed to solve in order to construct realistic models of the phenomenon.

The reported work is primarily an experimental investigation of the dynamic response of brittle materials under the conditions of uniaxial shock-wave compression. The final general goals are to provide the fundamental understanding and necessary experimental data for advancing the development of reliable, physics-based, multi-scale models, to provide a reliable foundation for the criteria of transitions from brittle response to ductile response under confining stresses, and to characterize the post-failure behavior of brittle materials. The experimental study was focused on the necessary conditions to initiate the failure waves in shock-compressed brittle materials and on the problem of steadiness of failure waves at different stresses.

With this goal we performed a comprehensive systematical experimental study of the failure wave phenomena in different kinds of brittle materials. We tested glasses of various hardness, brittle single crystals, and ceramics in order to distinguish contributions of matter hardness, homogeneity, and surface state into nucleation of compressive fracture. The principal experiments were plane wave experiments with relatively thick single sample plates and piles of plates of the same total thickness.

In modeling the behavior of materials subjected to intense impulsive loading, it is usually implied that local material response can depend only on characteristic material properties and the local state. In the case of cracking, the material ahead of the fracture zone should not "know" that cracks even exist. It seems that the failure wave is an example of non-local behavior. The response of each representative volume in the body depends not only on its local state, but also on whether the failure wave has approached the domain of influence. Based on the experimental data obtained, a computer simulation of the wave processes in shocked glass was performed. The goals of this part of the work were to check main ideas on which interpretation of experimental data is based, and to verify an analogy between a combustion wave and the failure wave.

2. Materials

The materials tested were four kinds of glass, two kinds of hard single crystals, and two kinds of ceramics. The glasses are listed in Table 1. Fused quartz is strongest glass of highest hardness whereas the heavy flint glass is the softest in this series. Since it was found earlier [2] that the shock-wave behavior of lapped glass plates is much more reproducible than that of as-received plates with mirror-like surfaces. In this study, the surfaces of glass plates were lapped with SiC powder of 40 μm grain size.

Other kinds of homogeneous brittle materials tested were quartz and silicon crystals. The quartz crystals were *x*-cut plates 40 mm by 40 mm in plane and 1.5 mm to 6 mm in thickness. Wackerly [3] and Fowles [4] studied dynamic compression of *x*-cut quartz and have found the HEL in the range of 5.5 to 6.5 GPa at the average propagation velocity of the elastic precursor front 5.95 km/s. The data on elastic shock compression along <100> axes are well described by the Hugoniot $U_s = 5.75 + 0.5\ u_p$ (km/s).

Table 1.

Glass	ρ, g/cm^3	c_l, km/s	Poisson's ratio, ν	Hugoniot elastic limit, GPa
Fused quartz	2.205	5.95	0.18	8.7
K8 crown glass	2.52	5.85–6.05	0.209	8 ± 1
TF1 heavy flint glass	3.86	4.04	0.227	3.1–4.7
Soda lime glass	2.45	5.72±0.08	0.23	8

The silicon samples of 3 to 6 mm in thickness were cut off a massive silicon block shown in Fig. 3 and were not specially oriented for the tests. All the sample plates were lapped in order to create conditions for nucleation the failure waves. Measured longitudinal sound speed in silicon plate in the impact direction is 8.82±0.02 km/s that is close to known value of 9.13 km/s in the direction <110>. Gust and Royce [5] measured the Hugoniot of silicon and have found for shocks along <110> axes the HEL equals to 5±0.5 GPa at the elastic precursor speed 9.49 km/s. Their data on elastic shock compression along <110> axes may be described by the Hugoniot $U_s = 9.15 + 1.45\ u_p$ (km/s).

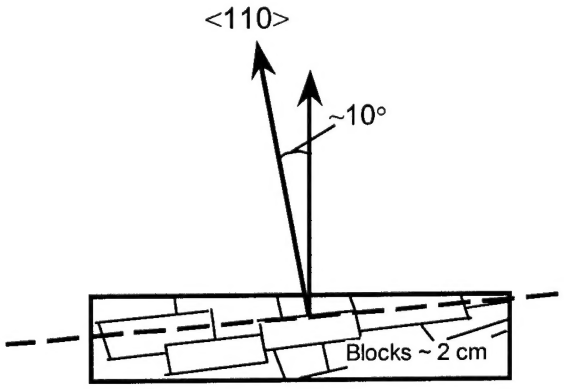

Figure 3. Structure and orientation of silicon block from which the samples were cut off.

Two hard ceramics were tested in order to reveal possible influence of internal non-uniformity of a matter on the failure wave phenomena. The ceramics were hot pressed alumina (96% purity) and boron carbide (97% purity) produced by Microceramica Ltd., Haifa, Israel with mechanical properties listed in Table 2. The main grain size of the ceramics was around 20 μm with smaller particles somewhere between grains. The samples were cut off from thicker plates using a diamond tool; the residual roughness of their surface was of order of 1 to 2 micrometers.

Table 2.

Ceramic	ρ, g/cm^3	c_l, km/s	c_s, km/s
Alumina	3.91–3.94	10.51–10.94	6.29–6.39
Boron carbide	2.31–2.49	10.79–13.98	7.62–8.85

3. Experimental Techniques

To investigate the strength properties of condensed matter under shock-wave loading we have to be able to create plane shock pulses in our samples and to measure an evolution of these pulses inside the sample. Plane shock waves were created by impacting the sample to be studied with a flyer plate. Figure 4 shows one of a typical arrangement of an explosive launching device. The impactor remains flat over its central part despite the fact that the pressure on the periphery of the explosive charge drops faster than on its axis because of the radial expansion of the explosion products. For this, the pressure pulse at the impactor edge is corrected by the guard ring. Due to reflection of the detonation wave from the guard ring, the pressure on the periphery rises for short time which produces additional inflow of the explosion products into the gap above the impactor. In our experiments we used aluminum impactor plates 2 mm to 7 mm in thickness which were launched by explosive facilities with velocities within a range of 0.9 km/s to 2 km/s.

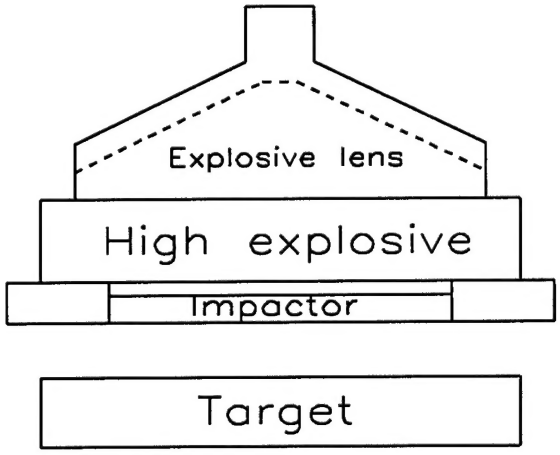

Figure 4. Experimental configuration for using explosives to launch a flyer plate.

The free-surface velocity profiles or the velocity histories of interface between the sample and some transparent "window" (water, PMMA, or LiF crystals) were recorded with the VISAR laser Doppler velocimeter shown in Fig. 5. The high space resolution of the laser techniques is due to the fact that the laser beam is focused down to a spot ~0.1 mm in diameter on the target surface. The output VISAR signals were recorded with a high-frequency digital oscilloscope at the sampling rate of 0.5 or 2.5 GHz (2 ns or 0.4 ns between points, correspondingly) and 500 MHz bandwidth (~1 ns time resolution). Additionally, several experiments have been carried out

where the stress histories were measured in shock-loaded samples with manganin piezoresistive gauges.

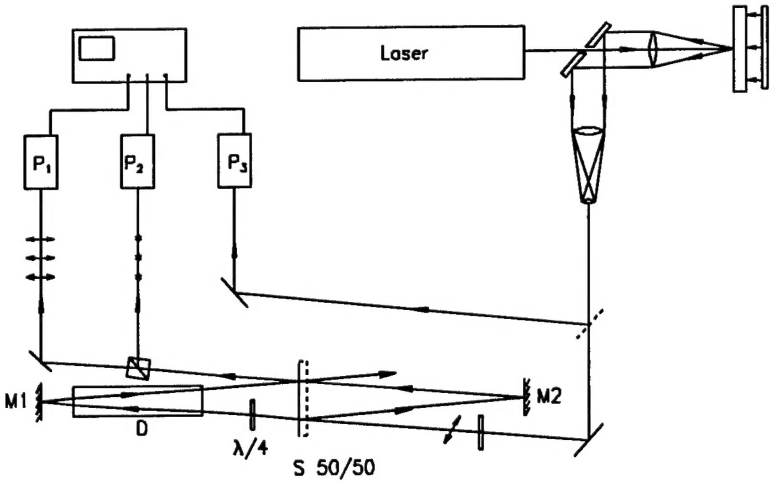

Figure 5. Schematic of a VISAR two-beam laser Doppler velocimeter [6].

Following the results of previous studies, main part of the measurements has been done in the experimental arrangements shown in Figs. 6*a* and 6*b*. The material of base plate was varied in order to vary the peak stress in the sample and the conditions of wave reflections at the interface. In the experiments with single sample plate we recorded general waveforms in the materials tested, and measured the Hugoniot elastic limit and the failure wave speed if the latter formed. The goals of experiments with piles of thin sample plates were to check whether the failure wave is formed in this material and to measure the failure threshold. Main part of the experiments has been done with free sample surfaces; some experiments on ceramics and single crystals were done with water or PMMA windows.

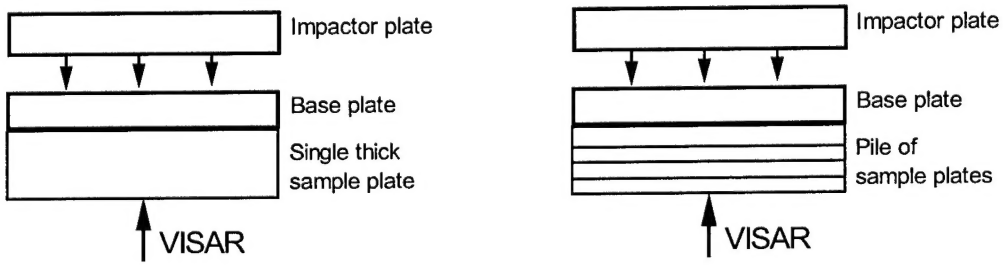

Figure 6. Scheme of the main experimental arrangements. In some experiments the velocity histories of interface between the sample and some transparent "window" (water, PMMA, or LiF crystal) were recorded with the VISAR instead of the free surface velocity histories.

For determining characteristic stress values, such as the peak stress or the Hugoniot elastic limit, the measured free surface velocity histories were transformed into the stress histories. For shock waves, the calculation was based on the Rankin-Hugoniot conservation equations and the assumption that the free surface velocity, u_{fs}, is doubled particle velocity u_p of shock-compressed matter: $u_{fs} = 2u_p$. When experiments with windows were interpreted, decompositions of shock discontinuities were analyzed (see Fig. 7) accounting for non-linear compressibilities of materials of the sample and the window.

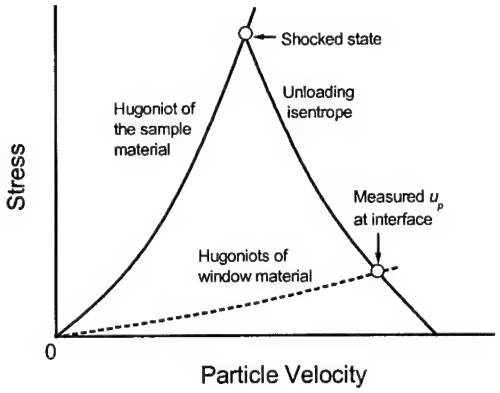

Figure 7. Decomposition of shock discontinuity at interface between the sample and the window.

Glasses often have anomalous compressibility in the elastic deformation region where the longitudinal sound speed decreases as the compressive stress increases. In this case the stress history was derived from the compressive parts of the free surface velocity profile with aid of the simple wave approximation. The compressive wave was considered as a simple centered wave described by a fan of characteristics. For simple waves the longitudinal stress increments is

$$d\sigma_x = \rho_0 a_\sigma du_p = \frac{1}{2}\rho_0 a_\sigma du_{fs} \tag{1}$$

where a_σ is the Lagrangian velocity of propagation of a part of the compression wave at the longitudinal stress σ_x [7] corresponding to the particle velocity u_p. For a centered simple wave the propagation velocity a_σ is

$$a_\sigma = c_l \frac{h/c_l}{h/c_l + t_\sigma} \tag{2}$$

where h is the sample thickness, and t_σ is the time interval after the elastic precursor wave front. Figure 8 presents example of such treatment of experiment with soda lime glass plate.

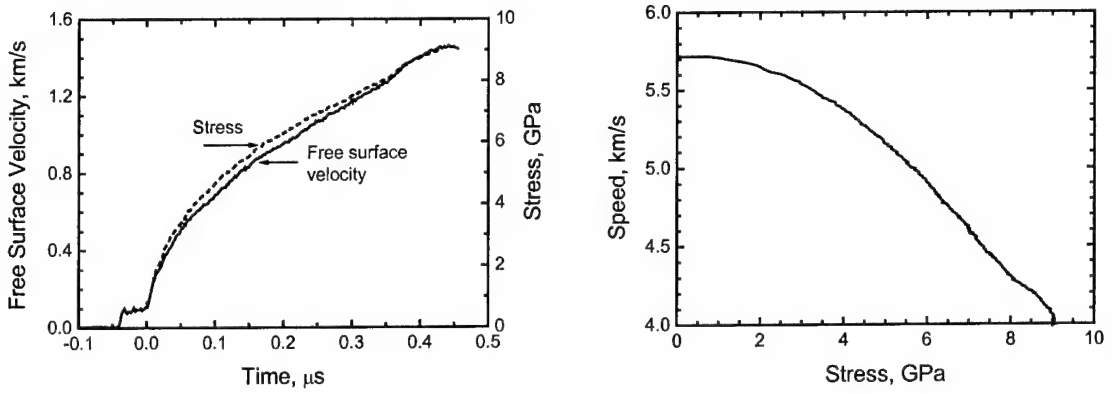

Figure 8. Compressive part of the free surface velocity history of a soda lime glass plate 5.9 mm in thickness impacted by aluminum flyer plate of 2 mm thick with the impact velocity being 1.90±0.05 km/s and calculated stress history and Lagrangian (substantional) wave propagation velocities.

4. Experimental Results

4.1. The failure wave speed in soda lime glass as a function of compressive stress

A series of shock-wave experiments with soda lime glass plates of different thickness have been performed with a goal to measure the failure wave velocities at various stresses and propagation distances. The measured free surface velocity histories are presented in Fig. 9. In Fig. 9 the time is normalized by the sample plate thickness in order to clearly compare the data. The free surface velocity histories display rounded compression wave front with a long rise time, which is due to an anomalous compressibility of this glass in the elastic region and a rate-dependent inelastic deformation above the elastic limit. The wave profiles in Fig. 9 contain small recompression pulses which are due to the wave reflection from a failed layer inside the sample. These recompression pulses are usually considered as a signature of the failure wave phenomenon.

Consideration of the time distance diagram shown in Fig. 1 demonstrates that the failure wave speed may be determined by means of measurement of the time interval t_r between arrivals of the initial compression wave and the recompression pulse fronts at the plate surface. The failure wave meets the unloading wave reflected from the glass free surface at the distance x and time moment t_x, as determined by the following relationships

$$t_r = 2\frac{\delta - x}{c_l}, \text{ and } t_x = \frac{\delta}{c_l} + \frac{\delta - x}{c_l} \tag{3}$$

where δ is the glass plate thickness. The propagation velocity of the failure wave is given by

$$c_f = \frac{x}{t_x} = c_l \frac{2 - c_l t_r/\delta}{2 + c_l t_r/\delta} \tag{4}$$

It follows from Eq. (4) that for constant speed of the failure wave the ratio t_r/δ should not depend on the plate thickness. The data in Fig. 9 show that the failure waves propagate with a constant speed, which depends on the stress and decreases with the latter. The process becomes unstable and obviously stops at stresses near the failure threshold of the soda lime glass which has been determined in [2] as ~4 GPa.

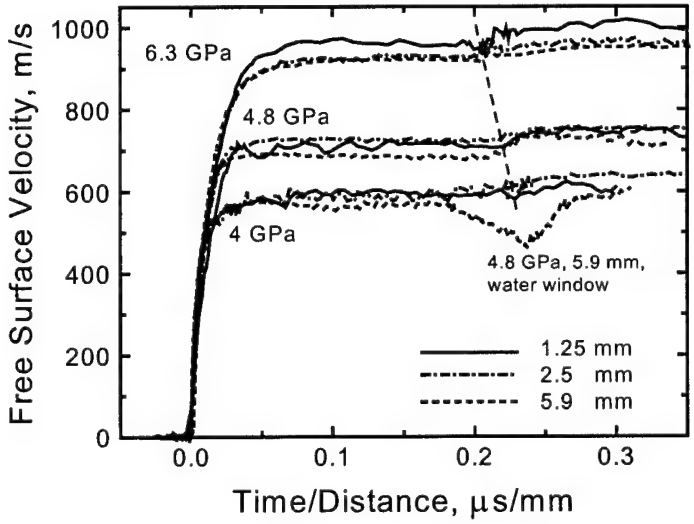

Figure 9. Free surface velocity histories of the soda lime glass plates of different thickness. The time is normalized by the sample plate thickness. The peak shock stresses are mentioned in the diagram. Dashed line notes the recompression waves (the velocity rise) that are the result of wave re-reflection at the failure front. One shot at 4.8 GPa and shorter load duration has been carried out with a water window.

Using the average value of 5.3 km/s for the sound speed we could find the failure wave speed decreases from 1.58±0.06 km/s at 6.3 GPa of compressive stress ahead of the failure front down to 1.35±0.06 km/s at 4 GPa. The uncertainty of the evaluation is mainly related to the dependence of longitudinal sound speed upon the stress. The stress dependence of the failure wave speed explains its apparent deceleration that was found in the first observations [8] of the failure waves where the glass samples were loaded by decaying stress pulses.

Figure 10 shows, in a larger scale, front parts of the free surface velocity histories measured for soda lime glass plates of different thickness at peak stresses of 4 GPa and 6.7 GPa. At both stresses the evolution of wave profiles, in general, everywhere close to that of a centered simple wave. On the other hand, the rounded transition from compression wave to plateau indicates that the response of glass is not purely elastic. Probably we have to account for internal friction in glass or other effects in order to understand this peculiarity.

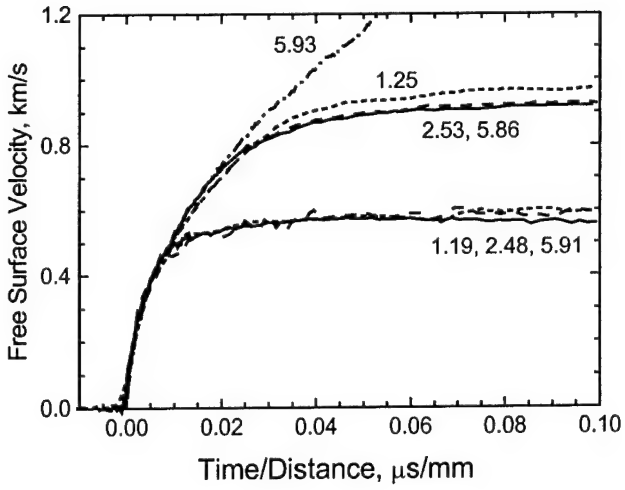

Figure 10. Profiles of compression wave of 4.1 GPa, 6.7 GPa and 9 GPa (dash-dot line) peak stress in soda lime glass plates of different thickness.

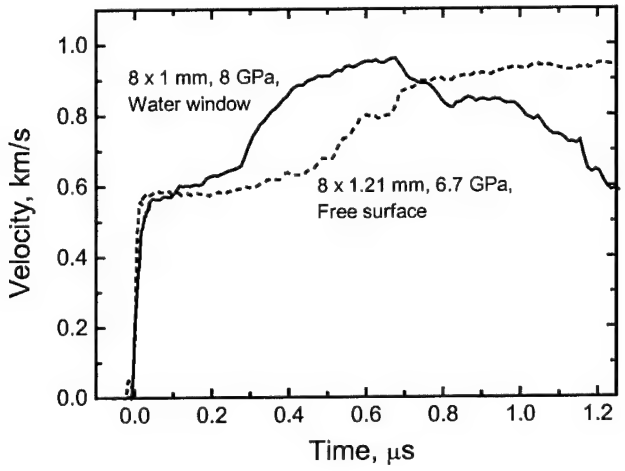

Figure 11. Results of two shots with piles of soda lime glass plates of different thickness at different peak stresses. The load duration at 6.7 GPa was approximately 1.5 times greater than that at 8 GPa.

Figure 11 presents the results of two shots with piles of soda lime glass plates of 1 and 1.21 mm in thickness at peak stresses of 6.7 GPa and 8 GPa. The data clearly demonstrate that (1) the failure threshold does not depend on the peak stress and thicknesses of the plates; (2) the rise

time of formed inelastic compressive wave is proportional to thickness of the plates; and (3) the velocity of propagation of inelastic compressive wave increases with increasing the peak stress.

4.2. Failure thresholds in different glasses

Figures 12 to 14 present the results of experiments with thick plates and piles of thin plates of fused quartz, TF1 heavy flint glass, and K8 crown glass, respectively, which demonstrate appearance of the failure waves in these materials. The rise time of the leading elastic wave in the piles is much less than the rise time in elastic wave propagating through a single thick plate. The reason of this disagreement is obviously associated with delays of propagation of compressive perturbations in porous interlayers between the lapped plates in the glass piles.

The failure waves nucleate on each surface of plates in the pile that results in decrease of stress at the front of elastic compression wave. If there are many plates in the pile, the stress magnitude at elastic wave front should approach the failure threshold. Thus estimated failure thresholds are 7.7 GPa for fused quartz (Hugoniot elastic limit is 8.7 GPa) and 5.3 GPa for K8 crown glass (HEL ≈ 8 GPa). In other words, there are very different relationships between the failure threshold and the Hugoniot elastic limit for soda lime glass, fused quartz, and K8 crown glass. In the case of softest TF1 glass, both the failure threshold and the HEL are not so certain, although the difference in responses of the thick plate and the pile of thin plates clearly indicates the failure process. It looks like the failure threshold is very close to the HEL value in this case.

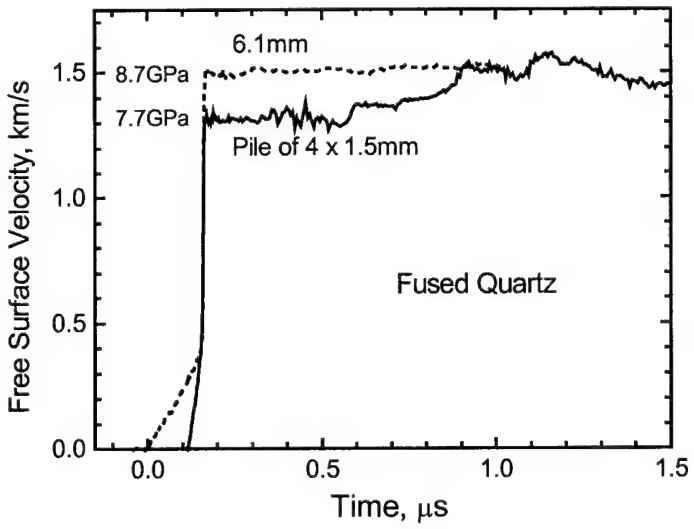

Figure 12. Results of experiments with thick plate and a pile of thin plates of fused quartz. Impact by aluminum flyer plate 4 mm in thickness with 1.5 km/s velocity.

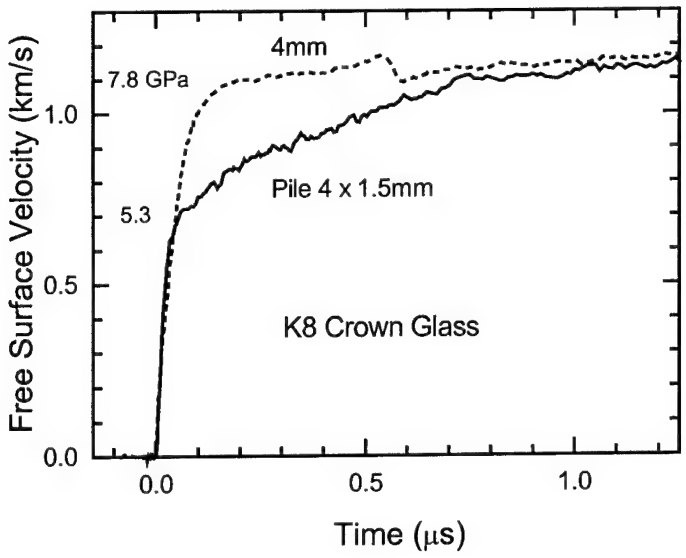

Figure 13. Free surface velocity histories of a thick plate and a pile of thin plates of K8 crown glass. Impact by aluminum flyer plate 7 mm in thickness with 1.15 km/s velocity.

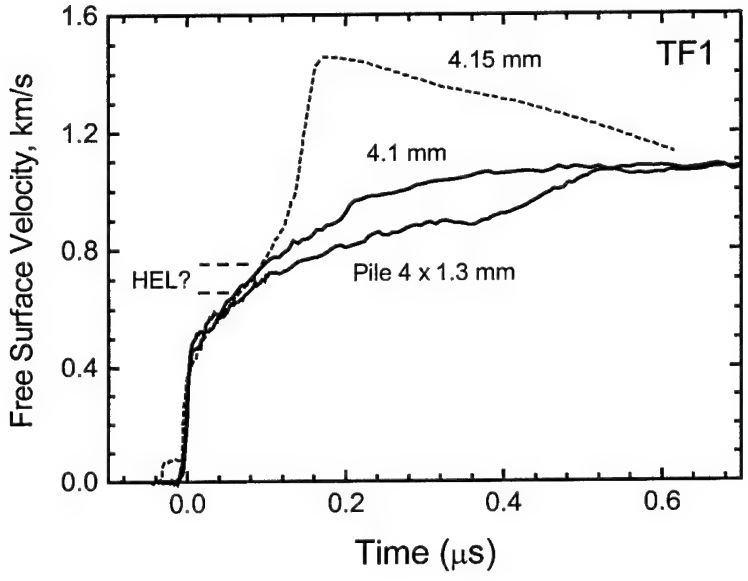

Figure 14. Free surface velocity histories of thick plates impacted to two different peak stresses and a pile of thin plates of TF1 heavy flint glass. Solid lines present results of experiments with shock loading by aluminum flyer plate 7 mm in thickness with 1.15 km/s velocity. Dashed line present the data at higher peak stress.

4.3. Verifying the failure wave formation in shock-compressed ceramics and hard single crystals

Figure 15 presents results of 2 experiments (2 shots) with thick plates and piles of thin plates of alumina ceramic, respectively. Reproducibility of the data is quite good. Unlike similar experiments with glasses, no evidence of the failure wave has been recorded. Instead of the decrease of the Hugoniot elastic limit in the pile as compared to the single plate, the data show its increase.

At the same total sample thickness, the time interval between the elastic precursor front and the "plastic' compressive wave is less for the pile than that for single plate. A reason of this discrepancy is obviously in that the plates in the piles had surface roughness of order of a few micrometers. This roughness creates thin gaps between plates. As a result, the total time of propagation of the elastic precursor front through the pile is a sum of the time of wave propagation through the plates and the time of closing these gaps. Since the wave speed is ~11 km/s while the speed of closing the gap is actually the free surface velocity at the HEL (300–400 m/s), even very thin gap markedly decrease the average propagation velocity of the elastic precursor front. The gaps become closed ahead the "plastic" compressive wave so the velocity of the latter in a pile is the same as in a single plate. Thus, the delay in arrival of the elastic precursor front, caused by the gaps, decreases the time interval between the elastic precursor front and the "plastic' compressive wave in the free surface velocity history.

The free surface velocity at the HEL is higher for piles than that for single plates. Probably this is an evidence of the precursor decay in alumina as a result of the stress relaxation behind the elastic front.

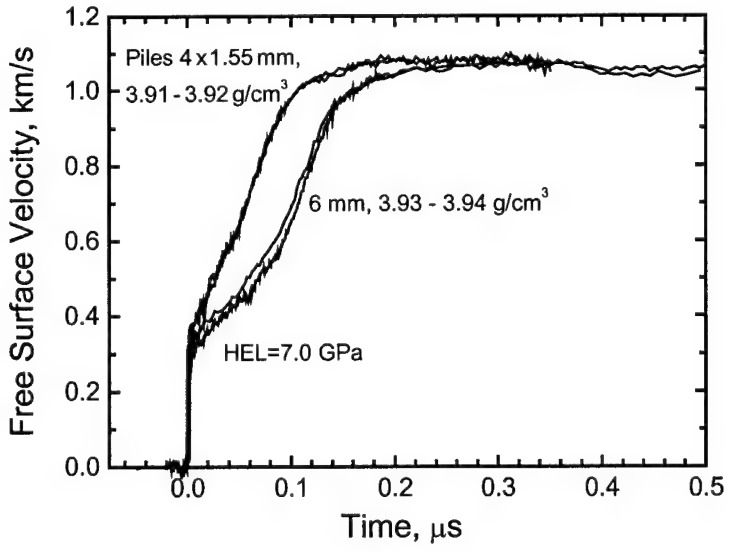

Figure 15. Free surface velocity histories of alumina samples composed of one plate 6 mm in thickness (two shots) and 4 plates 1.55 mm thick each (two shots). Impact by aluminum flyer plate 2 mm in thickness at 1.9 km/s velocity.

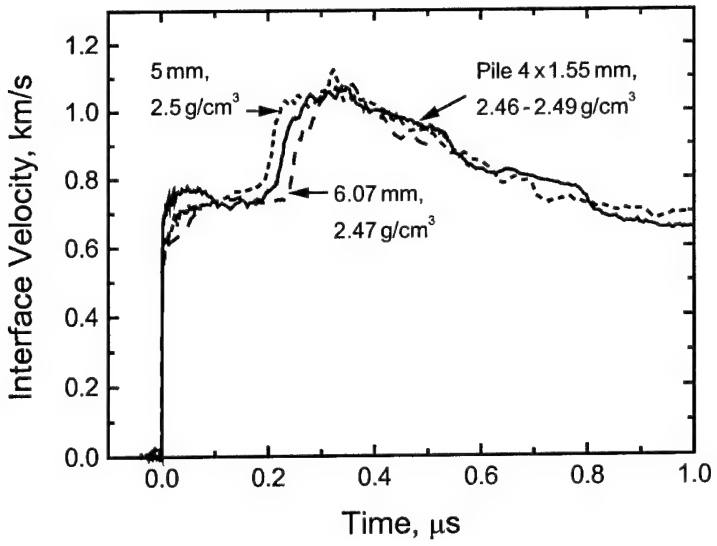

Figure 16. The interface velocity histories of boron carbide samples 5 mm and 6.07 mm in thickness (dashed lines) and a pile of four B_4C plates of 1.55 mm thick each (solid line). The material density was 2.46 g/cm^3 to 2.5 g/cm^3. Experiments with impact by aluminum flyer plate 2 mm in thickness at 1.9 km/s velocity using PMMA windows.

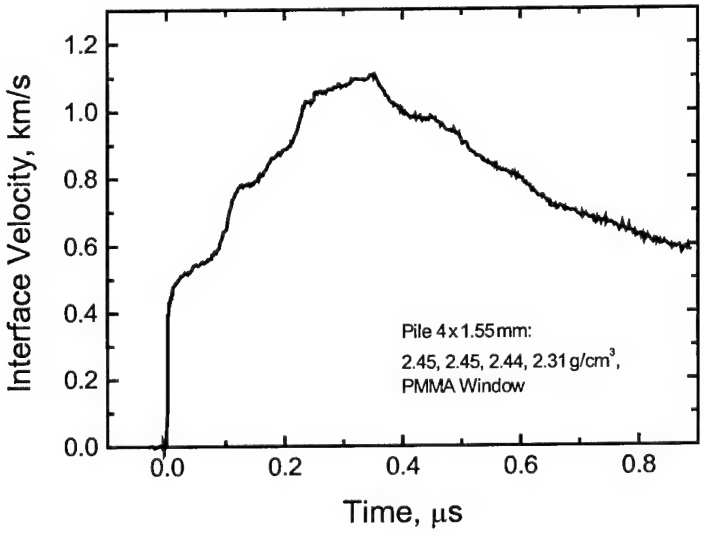

Figure 17. The interface velocity history of a pile of B_4C plates of 2.31 g/cm^3 to 2.45 g/cm^3 density. Experiment with PMMA window. The plate of lowest density was the last in the pile and contacted with the window.

The densities of boron carbide plates that we had for the experiments varied from 2.31 g/cm^3 to 2.5 g/cm^3. Figure 16 presents results of two shots with boron carbide plates 5 mm and 6.07 mm in thickness and one shot with a pile of 4 plates of a higher densities of 6.2 mm total thickness. Like in the experiments by Kipp and Grady [9], the waveforms are oscillated. Whereas there are many reasons to expect certainly brittle behavior of B_4C at shock compression, the wave profiles do not show any evidence of appearance of the failure wave in this material. The amplitude of elastic precursor wave even increased in the pile as compared to the single plates instead of expected decrease. Figure 17 presents the data for pile of B_4C plates of lower density 2.31 g/cm^3 to 2.45 g/cm^3. Even relatively small decrease in the density of ceramic resulted in large decrease in the HEL value.

Figure 18 presents the results of two experiments with quartz plates 6 mm thick and two shots with piles of four quartz plates 1.5 mm thick each. The waveforms are strongly oscillated, however one can certainly see that, again, the Hugoniot elastic limit is reproducibly higher for piles than that for single plates: the HEL is 5.3 GPa for 6-mm plates and 5.8 GPa for the piles of the same total thickness. Note also that the waveforms for piles are some less distorted by irregular oscillations than that for single plates. Obviously the oscillations are the results of strongly heterogeneous character of inelastic deformation with relatively large distances between localized shear bands or twins. We may probably suppose that interfaces in the piles suppress development of these shear bands and thus decrease the stress relaxation. Anyway, no evidence of the failure wave phenomenon in quartz single crystals are seen in presented wave profiles.

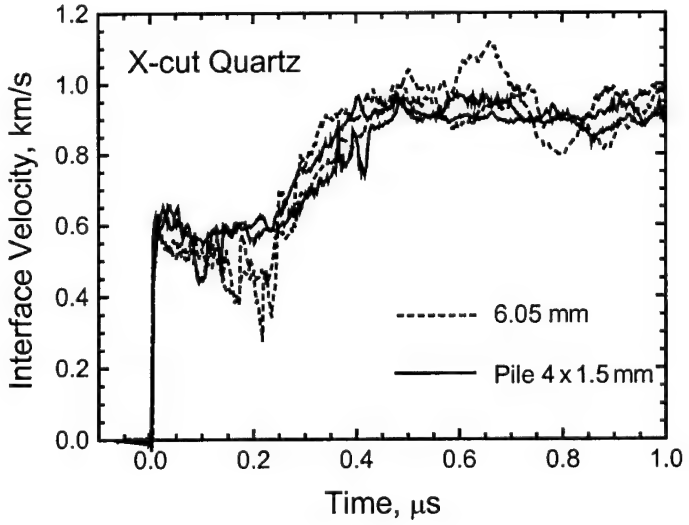

Figure 18. The interface velocity histories of thick x-cut quartz plates (dashed lines) and piles of thin quartz plates (solid lines) of the same total thickness. Measurements at interface between the sample and a water window. Impact by aluminum flyer plates of 7 mm in thickness with the velocity of 1.15 km/s.

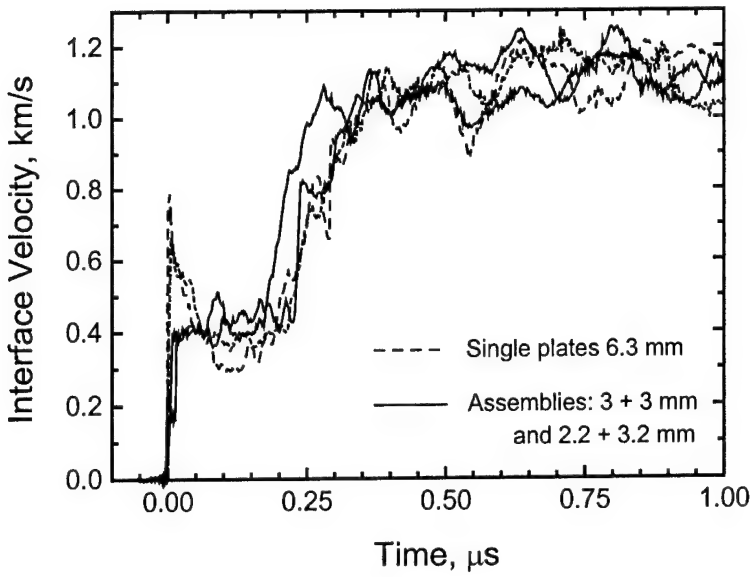

Figure 19. The interface velocity histories of thick silicon plates (dashed lines) and assemblies of two thin silicon plates (solid lines) of the same total thickness. Measurements at interface between the sample and a water window. Impact by aluminum flyer plates of 4 mm in thickness with the velocity of 1.5 km/s.

Figure 19 presents the results of four shots with silicon crystals. The velocity profiles for single plates are even more oscillated than that of quartz, nevertheless they distinctly show spike-like elastic precursor waves followed by the "plastic" compressive waves. The Hugoniot elastic limit, estimated as the stress at elastic spike is 7.7 to 9.5 GPa; behind the elastic precursor front the stress drops down to 3.5–4.3 GPa. Such large velocity decrement indicates high spall strength of the material behind the elastic wave front. When the thick samples have been replaced by assemblies of two thinner silicon plates, the shape of elastic precursor wave changed: instead of the spike the wave profiles exhibit almost rectangular precursor with 4.8 GPa stress at its front and some higher stress ahead of the "plastic" compression wave. By analogy with the glass piles, we could suppose that the observed decrease of HEL value in the assemble of plates is an evidence of the failure wave phenomenon in silicon crystals. However, it looks more possible that the effect is again just the result of delay in porous interlayer between the lapped plates.

4.4. Investigation of post-failure behavior of a glass.

Several attempts have been performed to obtain information about the post-failure states of shock-compressed glass and its compressibility in these states. The stressed state of shock-compressed glass could be evaluated by means of comparison of peak stress and specific volume, (σ_x, V), behind the failure wave with these values on an isentrope $p(V)$ of hydrostatic compression

of the glass like it was done for ceramics and sapphire [9, 10]. Unfortunately, besides the problems of accurate determining the σ_x and V values, we do not have any data on the bulk compressibility of glasses. Since it has been established that the failure waves in a pile of glass plates transform the compression wave to what is typical for elastic-plastic solids, it would be natural to try to recover the stress-strain diagram by means of Lagrangian analysis of compression and unloading waves [7].

Figure 20 presents an example of recording the stress histories in a glass pile. Unfortunately, we were not able to provide enough good quality and reasonable accuracy of these measurements. The gauges failed too rapidly. When we used thick insulating films to keep integrity of the gauges longer time, we got the signals which were too much distorted by the insulation and by the gaps between glass plates. Hence, more systematic efforts are required. Figure 21 presents results of measurements of the stress histories at interfaces between a pad of thin glass plates and copper barrier. In this arrangement the quality of records is much better. We hope to use these data in the future for evaluating the resistance to inelastic deformation of comminuted glass by means of computer simulations of the experiments.

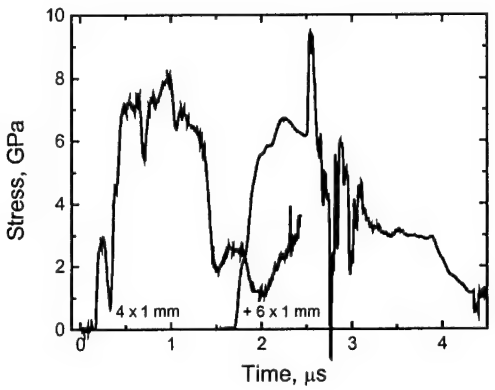

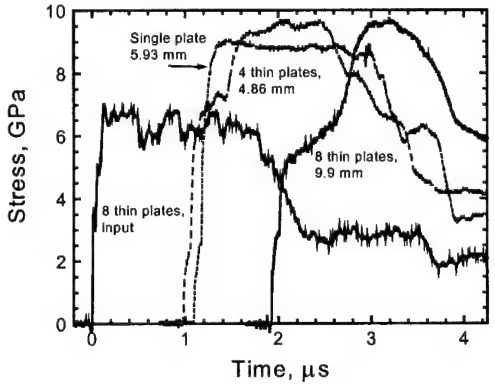

Figure 20. Stress histories in a pile of glass plates impacted by aluminum flyer plate 4 mm in thickness at the impact velocity 1.15 km/s. The pile was assembled of soda lime glass plates 1 mm thick on aluminum base plate 4 mm in thickness. Measurements with the manganin stress gauges which were insulated by Teflon films 100 μm from each side. First gauges was placed in 4 mm from the base plates, second gauges was 6 mm away from the first.

Figure 21. The stress histories at interfaces between a pad of thin glass plates and copper barrier.

Dynamic impedance of comminuted glass may be evaluated by means of measurements of the unloading way of shock-compressed glass which can be recovered from experiments with different windows. Figure 22 shows results of such experiments with soda lime glass plates 2.5 mm thick. These measurements provide the data about the unloading ways for the soda lime glass from the states ahead of the failure wave and behind it. The stress–particle velocity diagram shown in Fig. 23 indicates higher impedance of comminuted material than that of intact glass.

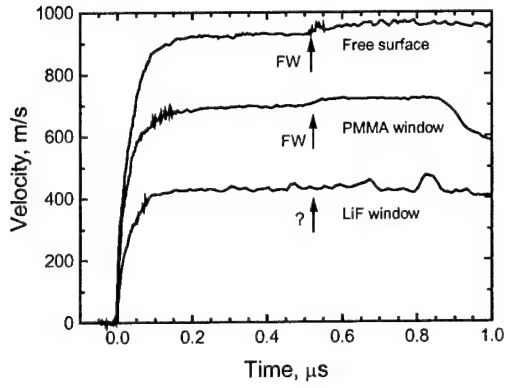

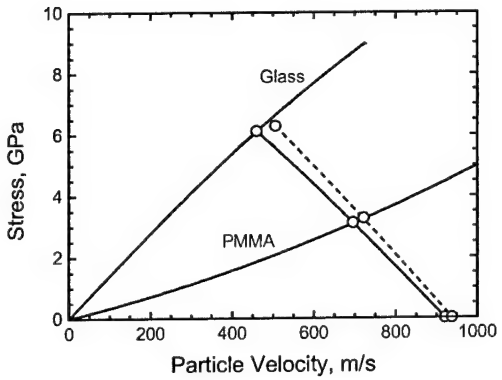

Figure 22. The velocity histories of free surface and sample/window interfaces of soda lime glass plates 2.5 mm in thickness at 6.3 GPa peak stress. Arrows show the recompression signal or the time moment when the recompression signal expected to appear.

Figure 23. The unloading ways of the soda lime glass from the states ahead of the failure wave and behind it.

5. Computer simulations of the failure wave phenomena.

A comprehensive model of the failure wave phenomena should include mechanisms and criteria of propagation of network of cracks, criteria and kinetics of the stress relaxation at cracking, and description of post-failure response of the material. Unfortunately, these problems are not enough clear yet. Nevertheless, we believe that even simplified versions of the failure wave model may be used now in order to verify main ideas and interpretation of observed effects.

Whereas the failure wave is really a wave process, its kinematics differs from that of elastic-plastic waves. The propagation velocity of the failure wave is determined by the crack growth speed which is not directly related to the matter compressibility. The glass surface plays an important role in the failure wave process because the surface is a source of cracks. In this sense the process is similar to diffusion. Experiments show that, when the stressed state is maintained, the subsonic failure wave propagates in a self-supported mode. Obviously the cracking creates new stress concentrations ahead of the cracking zone that in turn results in further cracking. In this sense there is an analogy with a subsonic combustion wave.

The simulations have been done in uniaxial geometry using one-dimensional Lagrangian code. We used some dimensionless parameter D ($0 < D < 1$) to describe the degree of damage of the material. $D = 0$ corresponds to undamaged state, whereas $D = 1$ is ascribed to completely damaged state and to states of thinnest surface layers of the material where the failure wave may occur. Following the analogy with combustion wave, expansion of a damaged layer wave at compressive stresses above the failure threshold, σ_f, was described by the wave equation

$$\left(\frac{\partial D}{\partial t}\right)_h = c_f \left|\frac{\partial D}{\partial h}\right|_t \qquad (5)$$

where c_f is the failure wave speed and h is the Lagrangian space coordinate. In order to provide smooth transition from purely elastic regime to appearance of the failure waves, c_f was presented as a saturating function of the compressive stress $\sigma_x > \sigma_f$:

$$c_f = c_c\left[1-\left(\frac{\sigma_f}{\sigma_x}\right)^6\right] \tag{6}$$

where $c_c = 1.6$ km/s is ultimate speed of a crack tip.

At each time moment and at each space point in a body a complete normal stress is presented as a sum of the hydrostatic pressure, p, (the mean stress) and the deviator stress, σ_d. When the material becomes failed the deviator stress relaxes to zero in accordance with the relaxation equation

$$\frac{\partial\sigma_d}{\partial t} = -\frac{\sigma_d}{\tau} \tag{7}$$

where τ is the relaxation time which depends on the damage:

$$\tau = \frac{\tau_0}{D} \quad \text{for} \quad 0 < D < 1; \;\; \tau_0 = 10^{-8} \text{ sec} \tag{8}$$

Actually, it was shown earlier [2] that the deviator stresses do not drop to zero in the failure wave. The behavior of comminuted matter also is more complex than just simple following to $p(V)$ hydrostat. On the other hand, real $p(V)$ hydrostats of glasses are not known yet. In our preliminary simplified simulations, we partly accounted for these circumstances by means of replacement of real $p(V)$ hydrostat by some equivalent linear dependence which is intermediate between bulk and longitudinal compressibilities. Although real compressibility of glass is anomalous and increases with stress, in these calculations it was assumed constant. Thus, the elastic behavior of glass was described by its longitudinal module $E' = 80$ GPa, whereas the states of comminuted matter were described by an effective module $K = 61$ GPa. The states of other materials involved into the calculations were described by their Mie–Grüneisen non-linear equations of state.

The results of all calculations presented below correspond to impact of a copper plate 5 mm in thickness at 0.65 km/s impact velocity upon a target consisted of one or several plates, including glass and other materials. The surfaces of each glass plate were potential sources of the failure waves that was realized by appropriation initial meaning $D = 1$ to the surface layer and $D = 0$ to the rest volume of glass. The code allows also an arbitrary amount of additional failure wave sources with $D = 1$ inside a glass plate.

Figure 24 presents results of simulation of the failure wave phenomenon in thick glass plate. The diagrams show that the combustion-like failure process really forms additional sub-sonic compressive wave. The recompression signal in the free surface velocity history is of much higher amplitude than the measured one but it appears at the same time moment.

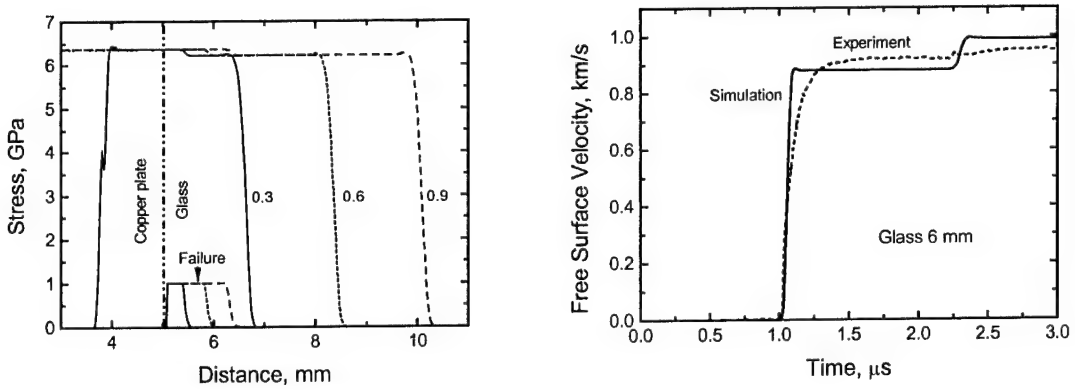

Figure 24. Results of simulations of combustion-like failure wave at shock compression of a glass plate 6 mm in thickness. The shock loading was created by collision of a thick copper plate with the sample glass plate. A Teflon film 0.06 mm in thickness was placed between the impactor and sample plates in order to simulate rough glass surface. In the stress-distance diagram the numbers indicate the time moments after impact (in microseconds), bottom part of the diagram shows expansion of the cracked zone.

Figure 25 demonstrate development of the wave process in a pile of 8 glass plates while Fig. 26 shows the free surface velocity history and the stress history at impact surface for this assemble. The simulation confirms that indeed the stress at leading elastic front decreases by steps each time when the elastic wave passes through contact between the glass plates where failure waves nucleate. After several plates passed the wave configuration is formed which consists of the leading elastic wave followed by a slower inelastic compressive wave.

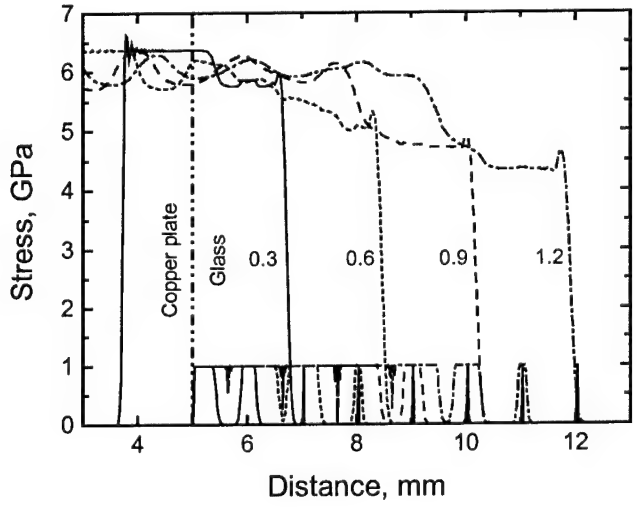

Figure 25. Results of simulations of compression wave in a pile of 8 glass plates.

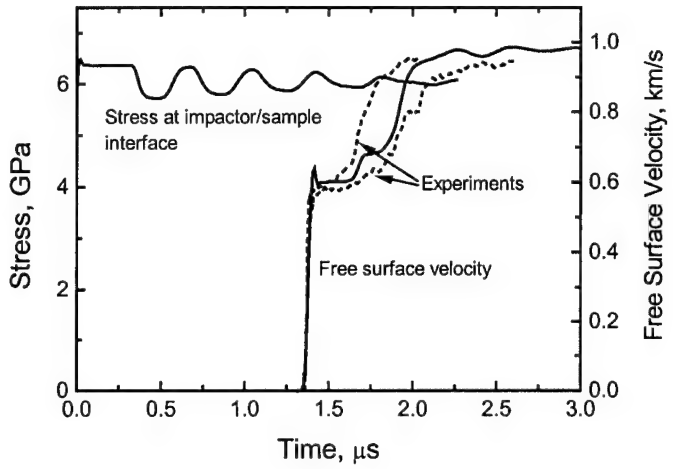

Figure 26. The stress history at interface between the copper impactor and the pile of 8 glass plates 1 mm thick each and the free surface velocity history of the pile. Results of computer simulations in comparison with experimental data from Fig. 11 for two piles of plates 1.0 and 1.2 mm thick.

Figure 27 compares the calculated and measured stress histories at interfaces between the impactor and the glass sample and between the glass sample and a copper barrier. Qualitatively, the simulations reproduce all main peculiarities of the experimental stress histories. It is interesting to note that the stress at barrier is higher for a pile of glass plates than that for a single thick glass sample plate as also observed in experiments shown in Fig. 21.

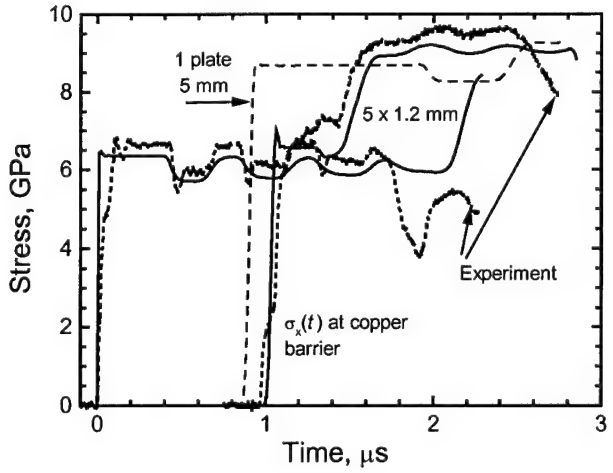

Figure 27. Calculated and measured stress histories at impactor/sample and sample/barrier interfaces. The sample was a pile of 5 glass plates 1.2 mm thick each. Additionally, the result of simulation for one glass plate 5 mm thick is shown.

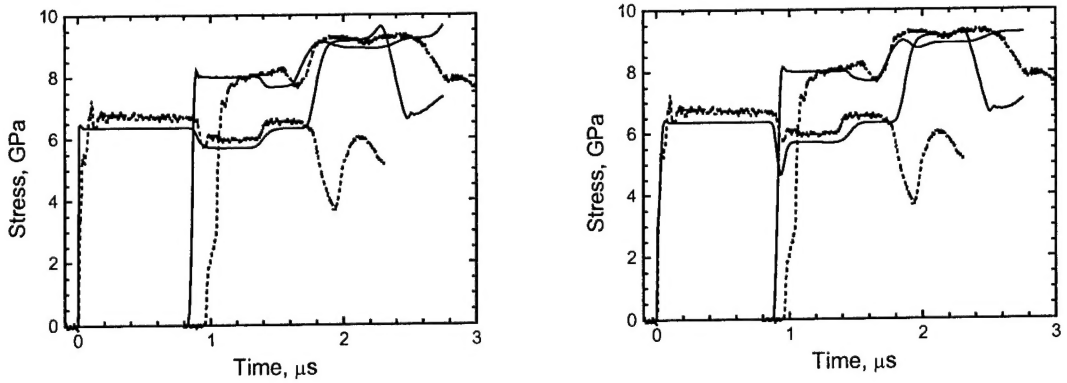

Figure 28. Influence of porous interlayers between glass plates on the stress histories. The samples were assembled of two glass plates 2.5 mm thick each. The porous interlayers were simulated by Teflon films 0.06 mm in thickness. Simulated and measured stress histories at input surface and at interface between the sample and a copper barrier are presented by solid and dashed lines, correspondingly.

In Fig. 28 calculated and measured stress histories are compared for the glass samples assembled of two plates. Since in experiments the surfaces of glass plates were lapped, the porous interlayers were simulated by Teflon films 0.06 mm in thickness. With this addition the simulations, again, well reproduce experimental stress histories. The results show that preceding unloading (which is created by interlayers) is not necessary condition for the failure wave process. In other words, the failure wave may accompanied by decrease in the stress as well as by its increase.

Conclusion

Shock-wave experiments with four glasses of different hardness, two ceramics, quartz and silicon single crystals have been carried out. Experiments with piles of thin sample plates confirm the appearance of the failure wave in elastically compressed fused quartz, K8 crown glass, and heavy flint glass, although the relationships between the Hugoniot elastic limits and the failure thresholds of these glasses are different. For softest heavy flint glass, the failure threshold is closest to the HEL. The failure waves were not recorded in single crystals and polycrystalline alumina and boron carbide ceramics. Thus it looks reasonably to assume that the failure wave may appear in a material body, the surface state for which differs much from that inside the body. Probably, the other necessary condition is certain relationship between the stress components. In accordance with the Griffith criterion the compressive failure starts when the tensile stress acting on the largest crack of the most vulnerable orientation exceeds some critical value that is reached when the criterion

$$(\sigma_1 - \sigma_2)^2 = Y_{brit}(\sigma_1 + \sigma_2)$$

is satisfied. In the case of uniaxial shock compression the transversal stress σ_2 is nonzero by definition and varies proportionally to the axial stress σ_1: $\sigma_2 = \sigma_1 \nu/(1-\nu)$. Probably, for single crystals the failure wave may be recorded at divergent shock loading.

The results show that the propagation speed of the failure wave in glass slightly depends on the stress above the failure threshold, and does not depend on the propagation distance. The stress dependence of the failure wave speed explains its apparent deceleration that was found in the first observations [8] of the failure waves where the glass samples were loaded by decaying stress pulses. The process becomes unstable and stops at stresses near the failure threshold. Longitudinal compressibility of comminuted glass has been found close to that of intact material.

An analogy between the failure wave and combustion wave has been tested by computer simulations of the experiments. Preliminary results demonstrate reasonable capabilities of the combustion-like model of failure wave.

References

1. G. I. Kanel, S. J. Bless. Compressive fracture of brittle solids under shock-wave loading. In: Ceramic Armor Materials by Design (eds. J.W. McCauley, A. Crowson, W.A. Gooch, A.M. Rajendran, S.J. Bless, K. Logan, M. Normandia, and S. Wax), *Ceramics Transaction*, **134**, 197-216
2. G.I. Kanel, A.A. Bogatch, S.V. Razorenov, Zhen Chen. Transformation of shock compression pulses in glass due to the failure wave phenomena. *J. Appl. Phys.*, **92**(9), 5045-5052 (2002).
3. J. Wackerle, Shock wave compression of quartz. *J. Appl. Phys.*, **33**, 922-937 (1962).
4. R. Fowles. Dynamic compression of quartz. *J. Geophys. Res.*, **72**(22), 5729-5742 (1967)
5. W.H. Gust and E.B. Royce. Axial yield strengths and two successive phase transition stresses for crystalline silicon. *J. Appl. Phys.* **42**(5), 1897–1905 (1971).
6. Asay, J.R. and L.M. Barker (1974). Interferometric measurement of shock-induced internal particle velocity and spatial variations of particle velocity. - *J. Appl. Phys.*, **45** (6), pp. 2540-254 (1974).
7. Fowles, R. and Williams, R.F. (1970). Plane stress wave propagation in solids. *J. Appl. Phys.*, **41**(1), 360-363
8. Kanel, G.I., Razorenov, S.V., and V.E. Fortov. The failure waves and spallation in homogeneous brittle materials. In: *Shock Compression of Condensed Matter 1991*, Ed.: S.C. Schmidt, R.D. Dick, J.W. Forbes, and D.G. Tasker, *Els.Sci.Publ.B.V.*, pp.451-454 (1992).
9. Kipp, M.E. and D.E.Grady. Shock compression and release in high-strength ceramics. In: *Shock Compression of Condensed Matter 1989.* Eds: S.C.Schmidt, J.N. Johnson and L.W. Davison. *Els. Sc. Publ. B.V.*, pp. 377-380 (1990).
10. Graham, R.A. and Brooks, W.P. Shock-wave compression of sapphire from 15 to 420 kbar. The effects of large anisotropic compression. - *J. Phys. Chem. Solids*, **32**, 2311-2330 (1971).

REPORT DOCUMENTATION PAGE

Form Approved
OMB No 074-0188

1. AGENCY USE ONLY (Leave blank)	2.REPORT DATE	3. REPORT TYPE AND DATES COVERED
	April 2003	Final, August 2002 - April 2003

4. TITLE AND SUBTITLE
A SYSTEMATIC STUDY OF THE FAILURE WAVE PHENOMENON IN BRITTLE MATERIALS

5. FUNDING NUMBERS
N62558-02-M-6020

.6. AUTHOR(S)
G.I.Kanel, A.A.Bogatch, S.V.Razorenov, A.S.Savinykh

7. PERFORMING ORGANIZATION NAME(S) AND ADDRESS(ES)
Institute for High Energy Densities of Russian Academy of Sciences
Izhorskaya, 13/19, Moscow, 127412 Russia

8. PERFORMING ORGANIZATION REPORT NUMBER

9. SPONSORING/MONITORING AGENCY NAME(S) AND ADDRESS(ES)

10. SPONSORING/MONITORING AGENCY REPORT NUMBER

11. SUPPLEMENTARY NOTES

12a. DISTRIBUTION/AVAILABILITY STATEMENT
Approved for public release; distribution unlimited

12b. DISTRIBUTION CODE

13. ABSTRACT ***(Maximum 200 Words)***

Shock-wave experiments with four glasses of different hardness, two ceramics, quartz and silicon single crystals have been carried out with the goals to better understand in which materials the failure wave may occur under shock compression, which material properties control the formation and propagation, and what are the threshold conditions. Experiments with piles of thin sample plates confirm the appearance of the failure wave in elastically compressed fused quartz, K8 crown glass, and heavy flint glass, although the relationships between the Hugoniot elastic limits and the failure thresholds of these glasses are different. For softest heavy flint glass, the failure threshold is closest to the HEL. The failure waves were not recorded in single crystals and polycrystalline alumina and boron carbide ceramics. The results show that the propagation speed of the failure wave in glass slightly depends on the stress above the failure threshold, and does not depend on the propagation distance. The process becomes unstable and stops at stresses near the failure threshold. Longitudinal compressibility of comminuted glass has been found close to that of intact material. Preliminary results of computer simulations demonstrate the potential of the combustion-like model in simulating the evolution of failure wave.

14. SUBJECT TERMS
Shock wave, failure wave, glasses, ceramics, quartz, silicon single crystals, failure thresholds

15. NUMBER OF PAGES
27

16. PRICE CODE

17. SECURITY CLASSIFICATION OF REPORT	18. SECURITY CLASSIFICATION OF THIS PAGE	SECURITY CLASSIFICATION OF ABSTRACT	20. LIMITATION OF ABSTRACT
UNCLASSIFIED	UNCLASSIFIED	UNCLASSIFIED	UL

NSN 7450-01-280-5500
Standart Form 298 (Rev.2-89)
Prescribe by ANSI Std. Z39-18
298-102